5222 *Chem. Mater.* **2010,** *22,* 5222–5234
DOI:10.1021/cm1012153

CHEMISTRY OF MATERIALS
Article

One-Pot Synthesis and Processing of Transparent, Conducting, and Freestanding Carbon Nanotubes/Polyaniline Composite Films

Rodrigo V. Salvatierra,[†] Marcela M. Oliveira,[‡] and Aldo J. G. Zarbin*[,†]

[†]*Departamento de Química, Universidade Federal do Paraná (UFPR), CP 19081, CEP 81531-990, Curitiba, PR Brazil, and* [‡]*Departamento Acadêmico de Química e Biologia, Universidade Tecnológica Federal do Paraná (UTFPR), Curitiba, PR Brazil*

Received April 29, 2010. Revised Manuscript Received July 19, 2010

In this work, we report for the first time, the synthesis of several carbon nanotube (CNT)/polyaniline (PANI) nanocomposites obtained through interfacial polymerization, in which the resulting material is obtained directly as a transparent and freestanding film at the water−toluene interface. The films are obtained spontaneously with high stability and can be easily transferred with high optical quality to any kind of substrate or directly to a desirable device. Samples containing several CNT/PANI ratios have been prepared. The characterization of the resulting materials was carried out by FT-IR, UV−vis-NIR, and Raman spectroscopy, X-ray diffraction, cyclic voltammetry, scanning and transmission electron microscopy, and conductivity measurements. The results indicate that the polymerization of aniline starts at the carbon nanotube walls, resulting in polymer-coated CNTs. A $\pi-\pi$ interaction between the CNTs and the PANI is proposed. The formation of the self-standing films is discussed in terms of the stabilization of the water−toluene interface.

Introduction

Interest in the preparation of nanocomposites of conducting polymers and carbon nanotubes (CNTs) has increased tremendously in recent years due to the synergistic effects resulting from the combination of these two classes of materials.[1−13] Among the conducting polymers, polyaniline (PANI) is one of the most studied due its environmental stability, ease of synthesis, low cost of the monomer, large conductivity range, and the different redox states that can be obtained: the fully reduced form leucoemeraldine (yellow), the half-oxidized form emeraldine (blue), and the fully oxidized form pernigraniline (purple).[14] Polyaniline can also be doped/dedoped by protonation, forming the so-called salt forms. The emeraldine salt (green) is the most conductive form of polyaniline.

Several studies have been conducted in recent years on the synthesis, characterization and applications of CNT/PANI nanocomposites. A dramatic improvement in the mechanical, thermal, electrical, optical, and redox properties of these nanocomposites is expected in comparison to their components individually. As a result, many possible applications in different devices have been described for these materials, for example, as sensors and biosensors,[15−17] as actuators,[18,19] in advanced biomedical devices,[20] in electronic devices,[21] in transistors,[22] as electrodes in batteries and supercapacitors,[23−26] as

*Corresponding author. Phone: +55-41-33613176. Fax: +55-41-33613186. E-mail: aldo@quimica.ufpr.br.

(1) Yan, X. B.; Han, Z. J.; Yang, Y.; Tay, B. K. *J. Phys. Chem. C* **2007**, *111*, 4125–4131.
(2) Baibarac, M.; Baltog, I.; Lefrant, S.; Mevellec, J. Y.; Chauvet, O. *Chem. Mater.* **2003**, *15*, 4149–4156.
(3) Li, L.; Qin, Z.-Y.; Liang, X.; Fan, Q.-Q.; Lu, Y.-Q.; Wu, W.-H.; Zhu, M.-F. *J. Phys. Chem. C* **2009**, *113*, 5502–5507.
(4) Zengin, H.; Z., W.; Jin, J.; Czerw, R.; Smith, D. W., Jr.; Echegoyen, L.; Carroll, D. L.; Foulger, S. H.; Ballato, J. *Adv. Mater.* **2002**, *14*, 1480–1483.
(5) Lafuente, E.; Callejas, M. A.; Sainz, R.; Benito, A. M.; Maser, W. K.; Sanjuan, M. L.; Saurel, D.; de Teresa, J. M.; Martinez, M. T. *Carbon* **2008**, *46*, 1909–1917.
(6) Wei, D.; Kvarnstrom, C.; Lindfors, T.; Ivaska, A. *Electrochem. Commun.* **2007**, *9*, 206–210.
(7) Dhand, C.; Arya, S. K.; Singh, S. P.; Singh, B. P.; Datta, M.; Malhotra, B. D. *Carbon* **2008**, *46*, 1727–1735.
(8) Wu, T.-M.; Lin, Y.-W.; Liao, C.-S. *Carbon* **2005**, *43*, 734–740.
(9) Garai, A.; Nandi, A. K. *Synth. Met.* **2009**, *159*, 1710–1716.
(10) Wu, T.-M.; Lin, Y.-W. *Polymer* **2006**, *47*, 3576–3582.
(11) Cochet, M.; Maser, W. K.; Benito, A. M.; Callejas, M. A.; Martinez, M. T.; Benoit, J.-M.; Schreiber, J.; Chauvet, O. *Chem. Commun.* **2001**, 1450–1451.
(12) Konyushenko, E. N.; Stejskal, J.; Trchova, M.; Hradil, J.; Kovarova, J.; Prokes, J.; Cieslar, M.; Hwang, J. Y.; Chen, K. H.; Sapurina, I. *Polymer* **2006**, *47*, 5715–5723.
(13) Gajendran, P.; Saraswathi, R. *Pure Appl. Chem.* **2008**, *80*, 2377–2395.
(14) de Albuquerque, J. E.; Mattoso, L. H. C.; Faria, R. M.; Masters, J. G.; MacDiarmid, A. G. *Synth. Met.* **2004**, *146*, 1–10.
(15) He, L. F.; Jia, Y.; Meng, F. L.; Li, M. Q.; Liu, J. H. *Mater. Sci. Eng. B* **2009**, *163*, 76–81.
(16) Lin, Y. H.; Cui, X. L. *Chem. Commun.* **2005**, 2226–2228.
(17) Li, M. Q.; Jing, L. H. *Electrochim. Acta* **2007**, *52*, 3250–3257.
(18) Mottaghitalab, V.; Xi, B. B.; Spinks, G. M.; Wallace, G. G. *Synth. Met.* **2006**, *156*, 796–803.
(19) Spinks, G. M.; Mottaghitalab, V.; Bahrami-Saniani, M.; Whitten, P. G.; Wallace, G. G. *Adv. Mater.* **2006**, *18*, 637–640.
(20) Ben-Valid, S.; Dumortier, H.; Decossas, M.; Sfez, R.; Meneghetti, M.; Bianco, A.; Yitzchaik, S. *J. Mater. Chem.* **2010**, *20*, 2408–2417.
(21) Ramamurthy, P. C.; Malshe, A. M.; Harrell, W. R.; Gregory, R. V.; McGuire, K.; Rao, A. M. *Solid-State Electron.* **2004**, *48*, 2019–2024.
(22) Lim, J. H.; Phiboolsirichit, N.; Mubeen, S.; Deshusses, M. A.; Mulchandani, A.; Myung, N. V. Nanotechnology **2010**, *21*, 075502.
(23) He, B. L.; Dong, B.; Wang, W.; Li, H. L. *Mater. Chem. Phys.* **2009**, *114*, 371–375.
(24) Sivakkumar, S. R.; Kim, W. J.; Choi, J.-A.; MacFarlane, D. R.; Forsyth, M.; Kim, D.-W. *J. Power Sources* **2007**, *171*, 1062–1068.
(25) Canobre, S. C.; Almeida, D. A. L.; Fonseca, C. P.; Neves, S. *Electrochim. Acta* **2009**, *54*, 6383–6388.

 Published on Web 08/13/2010

transparent and conducting thin films,[27] and in electrochemical devices,[28] among others.

One of the most important characteristics to be controlled in CNT/PANI nanocomposites is related to the polymer−nanotube interaction. The nature of the chemical and electronic interactions between the carbon nanotube and the polyaniline is responsible for the synergistic properties of the nanocomposites. In order to improve and to understand these properties, it is important to have an intimate contact (and an effective interaction) between both the components. The nature of the interactions between the CNTs and the PANI has been studied by different characterization techniques, such as Raman, UV−vis, and FT-IR spectroscopies, cyclic voltammetry, and thermal analysis, among others.[1−13,29,30]

Several synthetic procedures have been reported for the synthesis of CNT/PANI nanocomposites, such as the solid state mixing of both powder components, the mixture of dispersions of each component, and the electrochemical polymerization of aniline over a CNT-based electrode.[1−13] The in situ chemical polymerization of aniline in a dispersion of carbon nanotubes is the most successful route. However, the in situ polymerization route requires previous chemical treatment on the carbon nanotubes in order to guarantee the stability of their dispersion during the polymerization step. Different approaches to disperse the CNTs have been reported, including chemical functionalization of the nanotube walls (by acidic treatment, for example)[31] and the noncovalent adhesion of surfactants molecules.[32] The previous treatment of the CNTs plays an important role on the final characteristics (such as morphology) and properties (such as conductivity) of the nanocomposites obtained.[33]

Although the procedures to synthesize CNT/PANI nanocomposites have been successfully developed in recent years, the postsynthesis steps and the description of reproducible techniques to process these nanocomposites have not yet been achieved. For the majority of desirable applications, the nanocomposites need be processable as films that can be deposited over suitable substrates. For some important applications (for example, for the development of opto-electronic devices), these films need to be transparent. The most common routes described until now for the preparation of CNT/PANI nanocomposites yield insoluble powders that are difficult to disperse (and therefore unsuitable for most applications), although a few works described the preparation of soluble nanocomposites. For example, Sainz et al.[34] take advantage of the *n*-methylpyrrolidinone (NMP) solubility of the nonconducting emeraldine base form of polyaniline to prepare nanocomposites with CNTs, followed by film deposition by casting onto glass substrates, whereas Ma et al.[35] use single-stranded DNA to functionalize and solubilize the CNTs prior to the water-soluble nanocomposite preparation.

A very interesting approach to facilitate the polyaniline dispersion (and therefore the processability of the resulting nanocomposites) is the synthesis of polyaniline nanostructures; this approach makes possible the preparation of very stable colloidal dispersions. Kaner et al. have described an interesting approach to the synthesis of polyaniline nanofibers through interfacial polymerization.[36−39] It is a general chemical route based on a polymerization reaction performed in an immiscible aqueous/organic biphasic system, with the monomer aniline dissolved in the organic phase and the oxidant (generally ammonium persulfate) dissolved in the aqueous phase. The polymerization reaction starts at the interface (where the aniline contacts the oxidant), and subsequently, the resulting polymer migrates to the aqueous phase.[36] The interfacial polymerization avoids the successive steps of heterogeneous nucleation (responsible for the large particles of aggregates of polymer that are generally obtained by the one-phase traditional methods in the chemical oxidative synthesis of polyaniline), yielding small nanofibers that result in very stable water dispersions.[37]

During recent years, our research group has worked on the development of novel routes for the synthesis of different polyaniline-based nanocomposites.[40−46] We originally demonstrated the first in situ synthesis of a polyaniline/silver nanoparticle nanocomposite through interfacial polymerization;[43] through this process, different structures and morphologies of the nanocomposite could be obtained by rigorously controlling the reaction time.[43] In this work, we report for the first time the synthesis of several CNT/PANI nanocomposites obtained through interfacial polymerization. Using this process,

(26) Baibarac, M.; Gómez-Romero, P. *J. Nanosci. Nanotechnol.* **2006**, *6*, 1–14.
(27) Carroll, D. L.; Czerw, R.; Webster, S. *Synth. Met.* **2005**, *155*, 694–697.
(28) Li, L.; Ling, Q. D.; Zhu, C.; Chan, D. S. H.; Kang, E. T.; Neoh, K. G. *J. Electrochem. Soc.* **2008**, *155*, H205–H209.
(29) Kalbác, M.; Kavan, L.; Zukalová, M.; Dunsch, L. *Carbon* **2007**, *45*, 1463–1470.
(30) Lefrant, S.; Baibarac, M.; Baltog, I. *J. Mater. Chem.* **2009**, *19*, 5690–5704.
(31) Li, C.-C.; Lin, J.-L.; Huang, S.-J.; Lee, J.-T.; Chen, C.-H. *Colloid Surf. A* **2007**, *297*, 275–281.
(32) Bergin, S. D.; Nicolosi, V.; Cathcart, H.; Lotya, M.; Rickard, D.; Sun, Z.; Blau, W. J.; Coleman, J. N. *J. Phys. Chem. C* **2008**, *112*, 972–977.
(33) Coleman, J. N.; Khan, U.; Blau, W. J.; Gunko, Y. K. *Carbon* **2006**, *44*, 1624–1652.
(34) Sainz, R.; Benito, A. M.; Martinez, M. T.; Galindo, J. F.; Sotres, J.; Baro, A. M.; Corraze, B.; Chauvet, O.; Dalton, A. B.; Baughman, R. H.; Maser, W. K. *Nanotechnology* **2005**, *16*, S150–S154.
(35) Ma, Y. F.; Ali, S. R.; Wang, L.; Chiu, P. L.; Mendelsohn, R.; He, H. X. *J. Am. Chem. Soc.* **2006**, *128*, 12064–12065.
(36) Huang, J.; Kaner, R. B. *J. Am. Chem. Soc.* **2004**, *126*, 851–855.
(37) Li, D.; Huang, J.; Kaner, R. B. *Acc. Chem. Res.* **2008**, *42*, 135–145.
(38) Li, D.; Kaner, R. B. *J. Am. Chem. Soc.* **2005**, *128*, 968–975.
(39) Li, D.; Kaner, R. B. *J. Mater. Chem.* **2007**, *17*, 2279–2282.
(40) Schnitzler, D. C.; Meruvia, M. S.; Hummelgen, I. A.; Zarbin, A. J. G. *Chem. Mater.* **2003**, *15*, 4658–4665.
(41) Schnitzler, D. C.; Zarbin, A. J. G. *J. Brazil. Chem. Soc.* **2004**, *15*, 378–384.
(42) de Castro, E. G.; Zarbin, A. J. G.; de Oliveira, H. P.; Galembeck, A. *Synth. Met.* **2004**, *146*, 57–62.
(43) Oliveira, M. M.; Castro, E. G.; Canestraro, C. D.; Zanchet, D.; Ugarte, D.; Roman, L. S.; Zarbin, A. J. G. *J. Phys. Chem. B* **2006**, *110*, 17063–17069.
(44) Oliveira, M. M.; Ugarte, D.; Zanchet, D.; Zarbin, A. J. G. *J. Colloid Interface Sci.* **2005**, *292*, 429–435.
(45) Beleze, F. A.; Zarbin, A. J. G. *J. Brazil. Chem. Soc.* **2001**, *12*, 542–547.
(46) Maia, D. J.; De Paoli, M.-A.; Alves, O. L.; Zarbin, A. J. G.; Neves, S. d. *Química Nova* **2000**, *23*, 204–215.

Table 1. Experimental Conditions for the Synthesis of Samples[a]

sample	m CNT (mg)	V ani (μL)	m APS (mg)
PANI		60	38.6
CNTs/PANI-1/100	0.63	60	38.6
CNTs/PANI-1/32	0.63	20	12.8
CNTs/PANI-1/16	0.63	10	6.4
CNTs/PANI-1/8	0.63	5	3.2
CNTs/PANI-1/4	0.63	2.5	1.6
CNTs/PANI-0.5/8	0.31	5	3.2
CNTs/PANI-0.25/8	0.15	5	3.2

[a] m CNT = mass of carbon nanotubes; V ani = volume of aniline; m APS = mass of ammonium persulfate.

the resulting material is obtained directly as a transparent and freestanding film at the water−toluene interface. The films were obtained spontaneously with high stability and could be easily transferred with high optical quality to any kind of substrate or directly to a desirable device. We prepared samples containing several CNT/PANI ratios, and the interaction between the components was studied through different characterization techniques. In addition, we proposed a mechanism for film formation that may be extended to many other classes of nanocomposite materials. To the best of our knowledge, this study is the first report of the preparation of a CNT/PANI nanocomposite in which both the synthesis and processing are solved together in a one-pot reaction.

Experimental Section

Analytical grade toluene (Carlo Erba), acetone (Vetec), sulfuric acid (Merck), ammonium persulfate (Across), and trifluoroacetic acid (TFA, Vetec) were used as received. Aniline (Across) was bidistilled under vacuum before use. Water was deionized using a Milli-Q Ultra-Pure-Water Purification System.

The carbon nanotubes utilized in this work were prepared by CVD, starting from pure ferrocene, according our previous report.[47] The product resulting from this synthetic route is essentially formed by multiwalled carbon nanotubes filled by long crystals of iron-based species, mainly α-Fe, α-Fe_2O_3 (hematite), and Fe_3O_4. Some other carbonaceous species, such as carbon nanopolyhedra, are also present in small quantities in the sample. In order to guarantee higher stability in dispersion, the CNTs were previously treated with TFA according to the report by Chen et al.[48] Approximately 20.0 mg of CNTs was dispersed in a mixture of 50.0 mL of toluene and 5.0 mL of TFA. The dispersion was subsequently maintained under an ultrasound bath (Unique, 154 W, 37 kHz) for 2 h in an ice-bath (to avoid the TFA evaporation). The insoluble CNTs were then separated by centrifugation (3000 rpm for 5 min), washed three times with toluene, and three times with acetone, and dried at 50 °C.

Several CNT/PANI nanocomposites were prepared by varying the CNT/PANI ratio, as summarized in Table 1. All experiments were conducted at room temperature (between 21 and 24 °C). Five different CNT/aniline ratios (w/v) were used by fixing the CNT amount and varying the aniline volume: 1/100, 1/32, 1/16, 1/8, and 1/4. Two additional samples were prepared by fixing the monomer volume and varying the CNT mass: 0.5/8 and 0.25/8. For comparison, samples of neat polyaniline were also prepared according to exactly the same experimental procedure as that of the nanocomposites but without the carbon nanotubes. In all syntheses, the aniline/ammonium persulfate weight ratio was fixed at 1.6. The samples will be referenced here according the CNTs/aniline ratio employed in their preparation. For example, the sample **CNT/PANI-1/8** represents the nanocomposite prepared starting from a CNT/aniline weight/volume ratio of 1/8.

The preparation of the CNT/PANI nanocomposite was as follows: the correct amount of carbon nanotubes (see Table 1) is dispersed in 20 mL of toluene in an ultrasound bath for 40 min. Subsequently, the aniline is mixed in this dispersion using a micropipet, and the system remains under ultrasound for an additional 30 min. Then, the resulting mixture is transferred to a 50-mL round-flask containing 20 mL of a 1 mol L^{-1} H_2SO_4 aqueous solution in which a suitable amount of ammonium persulphate was previously dissolved (Table 1). The two-phase system is maintained under strong magnetic stirring (at 1500 rpm, using a magnetic stirrer from Corning and a stirrer bar of 5 mm in diameter × 15 mm in length) for 22 h. After a period of time, depending on the aniline concentration, a blue color appears, followed by a green color typical of the conducting form of the polyaniline, emeraldine salt. After 22 h, the magnetic stirring is stopped, and immediately a green and transparent film is spontaneously formed at the interface. To remove the excess acid and side products from the polymerization, all of the resulting material is transferred to a beaker. The aqueous phase is partially removed, and amounts of a diluted aqueous solution of H_2SO_4 (pH 6) are added to the system. This process in which the aqueous phase is constantly changed is repeated 10 times. In the same manner, the organic phase is constantly changed by successive removal of the toluene followed by additions of novel portions of toluene.

To deposit the nanocomposite films on substrates (glass slides of adequate size), cleaned substrates are placed into the beaker containing the biphasic system in which the film is at the interface. Then, using tweezers, the film is directly transferred to the substrate surface, followed by drying in air. The process of synthesis and film deposition of the CNT/PANI films is summarized in Figure 1.

The effect of stirring on the characteristics of the materials obtained was also studied. Samples were prepared according to the procedure described before but with the system at rest (Table 1). No films were obtained, and the nanocomposites were formed as insoluble powders deposited in the reaction flask. The solids were separated by centrifugation, washed several times with water, toluene, and acetone, and dried in air.

UV−vis spectra were collected directly from the films deposited on glass slides in a Shimadzu UV-2450 spectrophotometer, using air as the reference, in the range of 190−1100 nm.

X-ray diffraction measurements were done in a Shimadzu XD-3A diffractometer using Cu−Kα radiation, using 40 KV and 40 mA and at a 0.02° scan rate (in 2θ) with steps of 10 s per point. Powder silicon reflections were used for 2θ calibration. The samples were prepared by depositing the films directly over the aluminum sample-holder.

FT-IR spectra in attenuated total reflectance (ATR) mode were obtained using Bruker Vertex-70 equipment and an ATR accessory from Pike Technologies. The spectra were collected directly from the films deposited over the ZnSe crystal in the 4000−400-cm^{-1} range with 512 scans.

The Raman spectra were obtained in a Renishaw Raman Image spectrophotometer coupled to an optical microscope that

(47) Schnitzler, M. C.; Oliveira, M. M.; Ugarte, D.; Zarbin, A. J. G. *Chem. Phys. Lett.* **2003**, *381*, 541–548.
(48) Chen, H.; Muthuraman, H.; Stokes, P.; Zou, J.; Liu, X.; Wang, J.; Khondaker, S. I.; Zhan, L. *Nanotechnology* **2007**, *18*, 415606–415615.

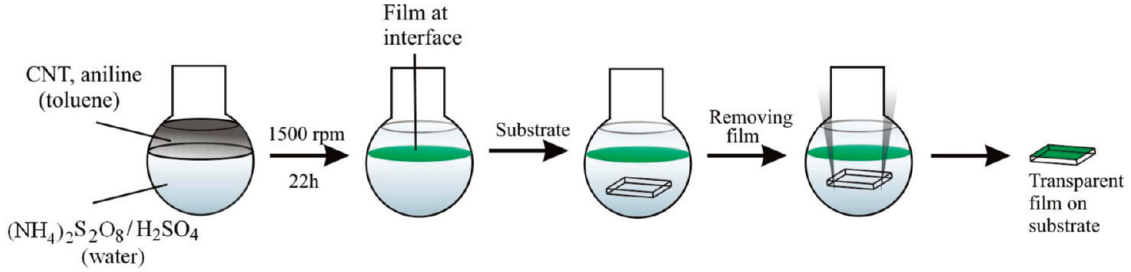

Figure 1. Schematic representation of the synthesis and deposition of CNT/PANI films.

focused the incident radiation down to a spot of approximately 1 μm. A He−Ne laser (emitting at 632.8 nm) and an Ar^+ laser (emitting at 514.5 nm) were used with an incidence potency of 0.2 mW over the 3000−200 cm^{-1} range.

The resistivity of the samples was measured directly from the films by the four-points technique using JANDEL Universal Probel equipment. The distance between the points was fixed at 1.0 mm. The films were deposited over planar glass substrates.

Thermogravimetric analyses (TGA/DSC) were carried out in SDT Q600 equipment (TA Instruments) under an atmosphere of synthetic air (White Martins, 100 mL min^{-1}) at a heating rate of 5 °C min^{-1}. The films obtained in the water/toluene interface were collected and powered to perform the analysis.

Transmission electron microscopy (TEM) was performed in a JEOL JEM 120 KV instrument. The samples were prepared by dropping a toluene dispersion of samples on standard copper grids covered by a thin film of amorphous carbon.

The scanning electron microscopy (SEM) images were obtained directly from the films deposited over a glass substrate using a Jeol JSM 6360 LV. A thin film of gold was deposited by sputtering over the films prior to measuring.

Cyclic voltammetry measurements were obtained using a micro-Autolab potentiostat (Eco-Chimie) that was interfaced to a PC computer and GPES 4.9 software. A one-compartment cell was used, with a Pt wire as counter electrode, an Ag/AgCl reference electrode, and a 0.5 mol·L^{-1} H_2SO_4 aqueous solution as the electrolyte. The work electrode was built by depositing the films obtained as described earlier over a ITO covered glass slide (active area = 1 × 1 cm). The scan speed was 20 mV·s^{-1}, and the potential ranged from −200 to 1000 mV.

Results and Discussion

According our previous report,[47] the CNTs used in this work were multiwalled carbon nanotubes filled with long crystals of iron-based species, mainly α-Fe, α-Fe_2O_3 (hematite), and Fe_3O_4. Other carbonaceous species were also present in small amounts. The previous treatment with TFA was employed for a better dispersion of CNTs in toluene. The chemical structure of the CNTs remained unchanged after the TFA treatment, as previously reported by Chen et al.[48] and corroborated by us. The characterization of the CNTs before and after the TFA treatment is available in Supporting Information (Figures S1−S5).

Figure 2 shows a photograph of the CNTs/PANI films deposited over round glass substrates. The transparency and optical quality of the films can be clearly observed. The green color of all the obtained films was the first evidence of polyaniline formation in its conducting form, emeraldine salt (ES). It is clear that the green color became less apparent and that the films became grayer

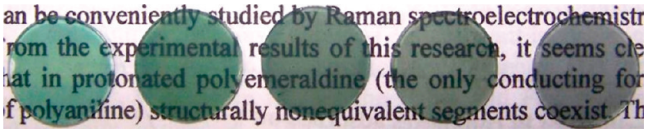

Figure 2. Photograph of the CNT/PANI films deposited over round glass substrates. The amount of CNTs in the films increases from left to right (samples **CNT/PANI-1/100**, **CNT/PANI-1/32**, **CNT/PANI-1/16**, **CNT/PANI-1/8**, and **CNT/PANI-1/4**, respectively).

as the CNT amount was increased (Figure 2, from left to right). Except when specifically mentioned, all of the characterizations discussed in the following were carried out directly from the films deposited, as illustrated in Figure 2.

The formation of polyaniline−emeraldine salt (ES) in all nanocomposite films was confirmed by Raman, FT-IR, and UV−vis spectroscopies as well as by cyclic voltammetry. In addition, these techniques gave important information regarding the CNT/polymer interactions.

Figures 3 and 4 show the Raman spectra of the nanocomposites in the 1000−3000-cm^{-1} region, which were collected using a laser emitting at both 514.5 nm (Figure 3) and 632.8 nm (Figure 4). The spectra of the neat polyaniline and neat CNTs are also shown for comparison. All the nanocomposite spectra show the bands attributed to the PANI-ES and the CNTs, confirming the occurrence of both of these components in the nanocomposites. The spectra of the neat CNTs (Figures 3g and 4g) are characteristic of multiwall carbon nanotubes (MWCNTs), presenting bands at approximately 1347 cm^{-1} (the so-called D band), 1575 cm^{-1} (G band), and a strong second-order Raman band at 2693 cm^{-1} (G′ band).[49] These bands are identified in the spectra presented in both Figures 3 and 4 as D, G, and G′, respectively.

The spectrum of the neat polyaniline collected with 514.5 nm shown in Figure 3a presents the following PANI-ES bands:[50−52] 1620 cm^{-1} (ν C−C of the benzene rings), 1586 cm^{-1} (ν C=C of the quinoid rings), 1516 cm^{-1} (ν C=NH^+ of the quinoid protonated di-imine units), 1485 cm^{-1} (ν C=N of the quinoid nonprotonated di-imine units), 1319 and 1340 cm^{-1} (ν C−N^+, characteristic bands

(49) Saito, R.; Jorio, A.; Samsonidze, G. G.; Dresselhaus, G.; Dresselhaus, M. S. *Nanotechnology* **2003**, *14*, 1130.
(50) Bernard, M. C.; Hugot-Le Goff, A. *Electrochim. Acta* **2006**, *52*, 595–603.
(51) Mazeikiene, R.; Tomkute, V.; Kuodis, Z.; Niaura, G.; Malinauskas, A. *Vib. Spectrosc.* **2007**, *44*, 201–208.
(52) Furukawa, Y.; Ueda, F.; Hyodo, Y.; Harada, I.; Nakajima, T.; Kawagoe, T. *Macromolecules* **1988**, *21*, 1297–1305.

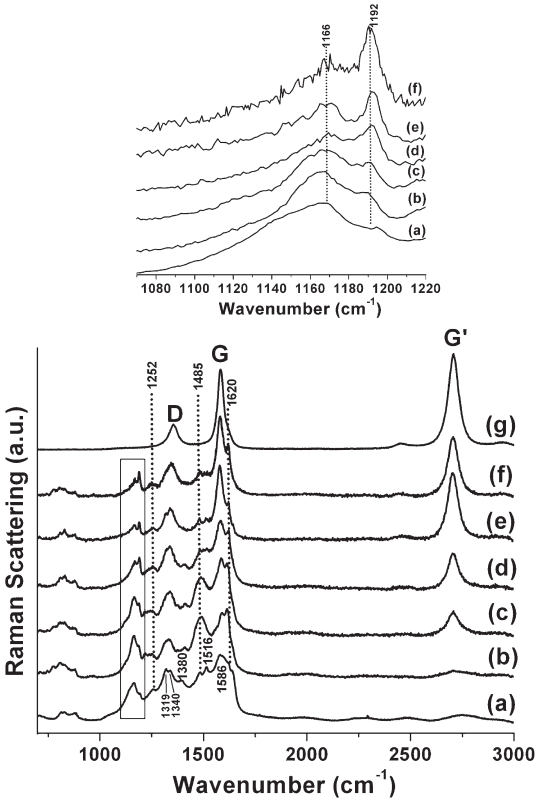

Figure 3. Raman spectra (λ = 514.5 nm) of the samples: (a) neat PANI, (b) **CNT/PANI-1/100**, (c) **CNT/PANI-1/32**, (d) **CNT/PANI-1/16**, (e) **CNT/PANI-1/8**, (f) **CNT/PANI-1/4**, and (g) neat CNTs. Inset: the details of the region characteristic of the C−H bending modes, marked with a rectangle in the figure.

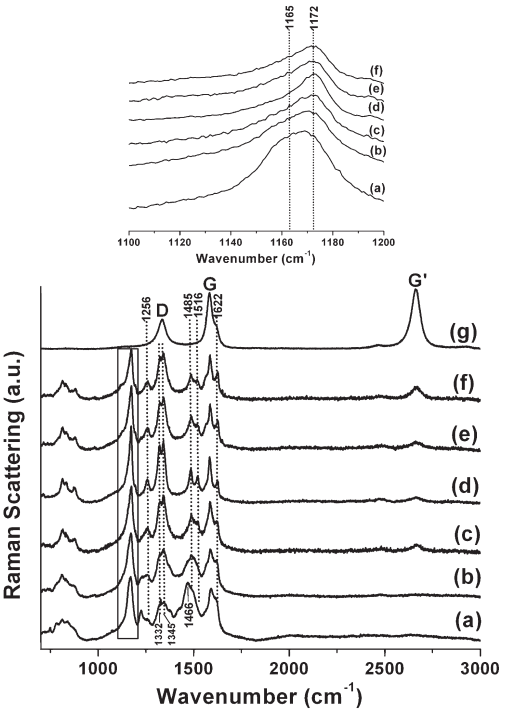

Figure 4. Raman spectra (λ = 632.8 nm) of the samples: (a) neat PANI; (b) **CNT/PANI-1/100**; (c) **CNT/PANI-1/32**; (d) **CNT/PANI-1/16**; (e) **CNT/PANI-1/8**; (f) **CNT/PANI-1/4**; and (g) neat CNTs. Inset: the details of the region characteristic of the C−H bending modes, marked with a rectangle in the figure.

of the polaron radical cation), 1252 cm^{-1} (ν C−N benzene diamine units), 1192 and 1166 cm^{-1} (C−H bending of the benzenoid and quinoid rings, respectively). It is clear that in the spectra of the nanocomposites films there is an increase in the relative intensity of the CNT bands according to the increase of the amount of CNTs (Figure 3b to f). The G′ band is a good indicator of this trend. Besides the confirmation of the presence of both the PANI-ES and the CNTs in the films, a closer look at the Raman spectra of the nanocomposites reveals important features regarding the polymer chain conformation and the CNT−polymer interaction. Some modifications of the bands attributed to the polyaniline can be clearly observed in response to the increase in the amount of CNTs in the nanocomposites: (i) the bands of polyaniline at 1166 and 1192 cm^{-1} are usually employed to verify the predominance of the kind of carrier (polarons or bipolarons) in the polymer lattice.[50] As we can see in the detail presented in the upper region of Figure 3, the increase in the amount of CNTs is accompanied by a significant increase in the relative intensity of the band at 1192 cm^{-1} (polarons, benzenoid rings) and vanishing of the band at 1165 cm^{-1} (bipolarons, quinoid rings), indicating that the presence of CNTs stabilizes the polaronic structure of PANI-ES; (ii) the bands at 1485 and 1516 cm^{-1} (ν C=N in quinoid rings, bipolarons) are collapsed and intense in the less-nanotube containing samples. Increasing the CNT amount causes a split and decrease of the relative intensity of these bands, which also indicates that the occurrence of bipolarons in the PANI-ES decreases according to the increase in the amount of CNTs in nanocomposites. In fact, it is noticeable that the relative intensities of these bands decreases proportionally to the increase of the intensity of the polaronic band at 1192 cm^{-1} discussed before; (iii) some modifications are seen in the polaronic bands at 1319 and 1340 cm^{-1}. However, the presence of the D band of the CNTs in this region makes any kind of conclusion regarding the effect of the CNTs over these bands difficult; (iv) a band of small intensity at 1380 cm^{-1} is observed in the spectra of the neat polymer and of the nanocomposites with smaller amounts of nanotubes (**CNT/PANI-1/100** to **CNT/PANI-1/16**). This band, attributed to the occurrence of tertiary nitrogen caused by the polymer reticulation,[53,54] is not seen in the spectra of the CNT-richest nanocomposites (**CNT/PANI-1/8** and **CNT/PANI-1/4**), indicating that the presence of CNTs induces the polymer chains to be less reticulated (and consequently more conductive); (v) an increase in the definition and intensity of the ν(C−C) band in benzenoid rings at 1620 cm^{-1}. All of these changes indicate the occurrence of a more conductive polyaniline, with an electronic structure more polaronic and rich in benzenoid rings when the amount of CNTs in the nanocomposites is higher.

The spectra collected with the 632.8-nm laser (Figure 4) present different profiles from that obtained with the

(53) Silva, J. E. P. d.; Faria, D. L. A. d.; Torresi, S. I. C. d.; Temperini, M. L. A. *Macromolecules* **2000**, *33*, 3077–3083.
(54) Šeděnková, I.; Trchová, M.; Stejskal, J. *Polym. Degrad. Stab.* **2008**, *93*, 2147–2157.

514.5-nm laser due to the resonance effect caused by the coincidence between a visible absorption band of PANI (assigned to the radical cation segment) and the laser energy.[55] For this reason, the intensity of the bands attributed to modes corresponding to the oxidized portions of the polymer is strongly enhanced. This resonance effect also makes the bands due to the polymer very salient in comparison to the CNT bands, such that only in the more CNT-concentrated samples can the CNTs bands be observable (see Figure 4). The effect of the CNT amount on the PANI-SE bands is also observed in these spectra, in a similar way as previously discussed: (i) the band at 1165 cm^{-1} in the neat polymer (C−H bending of the quinoid rings, bipolarons) are shifted to 1172 cm^{-1} with increasing amounts of CNTs in the nanocomposites (C−H bending of the benzenoid rings, polarons), as can be seen in the inset of Figure 4; (ii) the intensity of the band at 1485 cm^{-1} decreases, and the band at 1516 becomes apparent, indicating a more-conductive form of the PANI-ES; (iii) the band at 1622 cm^{-1} (ν(C−C) in benzenoid rings) becomes more defined; (iv) the band at 1466 cm^{-1} present in the neat polymer is not detectable in the spectrum collected with the 514-nm laser. This band is also attributed to the ν C═N in quinoid rings[11,54] and disappears in the samples containing higher amount of CNTs; (v) the relative intensity of the polaronic bands at 1332 and 1345 cm^{-1} is lower in the neat polymer and increases significantly in the nanocomposites.

The low-frequency region of the Raman spectra (200−1000 cm^{-1}) is very sensitive to the structure and conformation of the polyaniline chains.[56] The spectra of the samples obtained in this region, collected with the 632.8-nm laser, are shown in Figure 5. It is clear that the polymer bands are narrowest in the samples containing higher amounts of CNTs (Figure 5d−f), showing more uniformity in the energy of the related vibrational modes and consequently more uniformity in the polymer structure.

According to Colomban et al.,[56] the occurrence of the bands at 204 and 297 cm^{-1}, both related to the C_{ring}-N-C_{ring} angular deformation, is an indication that the polyaniline presents a pseudo-orthorhombic crystalline structure characterized as ES-I (emeraldine-salt type I). It is evident that an increase in the intensity of these bands (mainly the band at 297 cm^{-1}) occurs according to the increase in the amount of CNTs in the nanocomposites. Other features observed in the Raman spectra presented in Figure 4 show that the presence of CNTs affects the polymerization and induces a more-organized and planar PANI structure: (i) the bands at 420 and 527 cm^{-1} in the spectrum of neat PANI (Figure 4a) are attributed to the C−C out-of-plane deformation modes and are very sensitive to conformational changes in the polymeric chains.[56] These bands are shifted to 400 and 520 cm^{-1}, respectively, by the increase in the amount of CNTs in the nanocomposites. According to theoretical and experimental studies,[56,57] the lower position of these bands indicates smaller torsion angles in the polyaniline chains, which means that the CNTs induce the conformation of PANI with more planar chains; (ii) the bands at 812, 835, and 878 cm^{-1} are attributed to out-of-plane C−H motions and are very sensitive to the torsion angle between two aniline rings.[57] All three modes are clearly observed in the samples containing higher amounts of CNTs, corroborating the model in which the CNTs induce the occurrence of more-planar polyaniline chains. These modes are less defined and broader in the spectra of the neat polymer and of the sample **CNT/PANI-1/100** (the band at 878 cm^{-1} is not detectable in these spectra), suggesting a mixture of various torsion angles in the absence of significant amounts of CNTs.

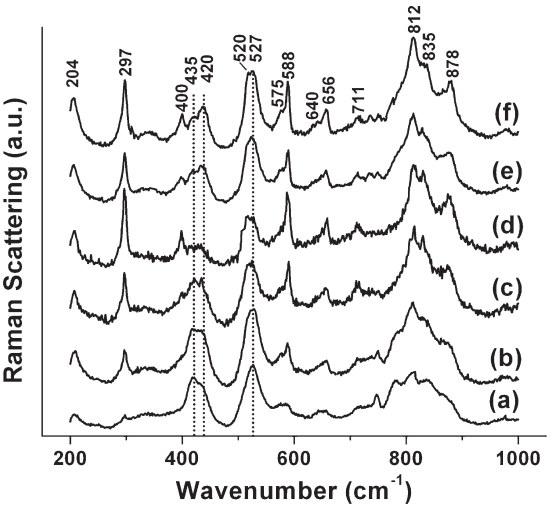

Figure 5. Low-frequency Raman spectra (λ = 632.8 nm) of the samples: (a) neat PANI; (b) **CNT/PANI-1/100**; (c) **CNT/PANI-1/32**; (d) **CNT/PANI-1/16**; (e) **CNT/PANI-1/8**; and (f) **CNT/PANI-1/4**.

The interpretations of the Raman data discussed before indicate that the CNT walls interacts with the polymer, stabilizing the polaronic structure of the doped polyaniline, probably through a $\pi-\pi$ interaction (between the delocalized electrons of the CNTs and the aromatic rings of the PANI). A more planar conformation of the polyaniline chains is assumed to be achieved according to the increase in the amount of CNTs in the nanocomposites.

The conclusions obtained by Raman spectroscopy were corroborated by FT-IR spectroscopy. In order to obtain the FT-IR spectra directly from the films of the samples (exactly as used to collect the Raman spectra), they were collected using the attenuated total reflectance (ATR) technique. The spectra are shown in Figure 6. The typical bands of PANI-ES are detectable in the spectra of the neat polymer and all the nanocomposites:[52,58] 1080 cm^{-1} (ν C−N^{+}═C), 1240 cm^{-1} (ν C−$N^{+\bullet}$ due to the radical

(55) Silva, J. E. P.; Temperini, M. L. A.; Torresi, S. I. C. *Electrochim. Acta* **1999**, *44*, 1887–1891.
(56) Colomban, P.; Folch, S.; Gruger, A. *Macromolecules* **1999**, *32*, 3080–3092.
(57) Cochet, M.; Louarn, G.; Quillard, S.; Buisson, J. P.; Lefrant, S. *J. Raman Spectrosc.* **2000**, *31*, 1041–1049.
(58) Louarn, G.; Lapkowski, M.; Quillard, S.; Pron, A.; Buisson, J. P.; Lefrant, S. *J. Phys. Chem.* **1996**, *100*, 6998–7006.

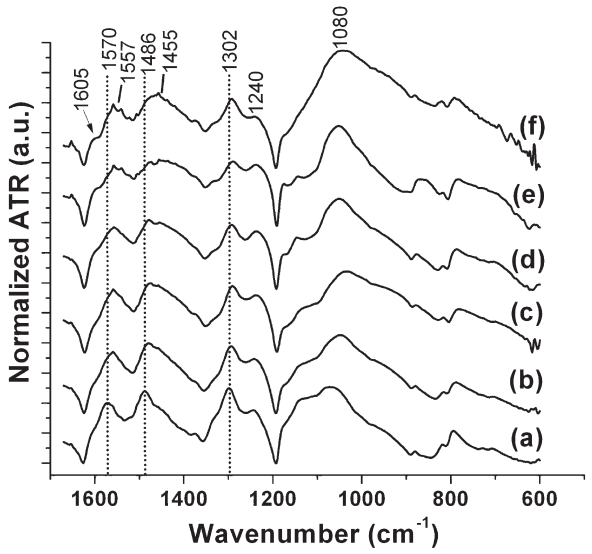

Figure 6. Normalized FT-IR spectra collected in attenuated total reflectance mode of the samples: (a) neat PANI; (b) **CNT/PANI-1/100**; (c) **CNT/PANI-1/32**; (d) **CNT/PANI-1/16**; (e) **CNT/PANI-1/8**; and (f) **CNT/PANI-1/4**.

cation), 1302 cm^{-1} (ν C−N in delocalized polarons), 1486 cm^{-1} (ν C−C in benzenoid rings) and 1570 cm^{-1} (ν C−C in quinoid rings). The ratio between the intensity of these two latter bands is usually employed to estimate the oxidation degree of the polymer.[52]

The degree of the doping in the PANI-ES has a well-known effect on the bands at 1080, 1486, and 1570 cm^{-1}. According to the increase in the doping degree, these bands are red-shifted, and the intensity of the band at 1486 cm^{-1} (benzenoid rings) is increased in relation to the band at 1570 cm^{-1} (quinoid rings) due to the larger formation of polarons in the polymer chains.[59] These effects are clearly observed in the CNT/PANI nanocomposite spectra according to the increase in the amount of CNTs, which means that the more conductive (polaronic) PANI is obtained in the samples containing higher amounts of CNTs.

The conclusions obtained by vibrational spectroscopy are also corroborated by UV−vis spectroscopy (see Figure S6, Supporting Information). The spectrum of the neat polyaniline presents all the typical bans of PANI-ES at 3.2 eV (due to the transitions from the valence band to the conduction band), 2.7 eV (the transition from the polaronic band to the conduction band), and 1.6 eV (the transition from the valence band to the polaronic band). All of these bands are also present in the nanocomposite films, but the polaronic bands are red-shifted according to the increase in the amount of CNTs in the samples (from 1.6 eV in the neat PANI to 1.4 eV in the sample **CNT/PANI-1/4**). This red shift is typical of more conductive polymers and is due to the increase in the delocalization of polarons resulting from the increase in the CNT amount in nanocomposites.

Figure 7 shows scanning electron microscopy (SEM) images of neat PANI, neat CNTs, and the CNTs/PANI nanocomposites, obtained directly from the deposited films illustrated in Figure 2. The neat polyaniline film is rough and continuous (Figure 7a). A close look at this film shows clearly that the film is composed of agglomerates of short polyaniline nanofibers, comparable to those produced by interfacial polymerization reported in literature.[36,37] This morphology is maintained in the films of the samples containing lower amounts of CNTs (**CNTs/PANI-1/100**, Figure 7b), in which some isolated CNTs can be seen embedded into the polymer continuum. The polymer morphology remains unchanged in the sample **CNTs/PANI-1/32** (Figure 7c); however, the amount of CNTs is much higher in the nanocomposite. It is clear that the CNTs observed in Figure 7c are larger in diameter and present more surface roughness in comparison to the neat CNTs (Figure 7g), which indicates that the CNTs are capped by a polymer shell.

The morphology of the CNT/PANI nanocomposites is totally modified in the samples containing higher amounts of CNTs. The SEM images of the samples **CNTs/PANI-1/16**, **CNTs/PANI-1/8**, and **CNTs/PANI-1/4** are shown in Figure 7d, e, and f, respectively. The continuum of the polymer (in which the CNTs were dispersed) observed in the previously described samples disappeared in the samples containing high amounts of CNTs. Otherwise, these films are formed basically by the interconnection of long fibers corresponding to polymer-capped CNTs. The roughness of the fiber surface is a clear indicator that the polyaniline was synthesized around the CNTs. The thickness of the fibers is reduced from the samples **CNTs/PANI-1/16** to **CNTs/PANI-1/8** to **CNTs/PANI-1/4**, which means that with the increased amount of CNTs (maintaining a fixed aniline amount), the polymer shell around the CNTs becomes thinner. The inset in Figure 7d clearly shows the capped CNTs and some CNTs in which the capping process failed (resulting in half-capped CNTs, indicated by arrows in the inset of Figure 7d).

The TEM images of selected nanocomposite samples confirm the polymer capping around the isolated CNTs. Figure 8a shows the TEM image of the film of neat polyaniline, showing the fibrilar structure characteristic of polyaniline obtained through interfacial polymerization. Figure 8b shows the TEM images of the **CNTs/PANI-1/100**, and Figure 8c shows the TEM images of the sample **CNTs/PANI-1/32**. In the sample with less CNTs (**CNTs/PANI-1/100**), the occurrence of aggregates of polyaniline nanofibers, with isolated CNTs dispersed along them is clear (Figure 8b). By increasing the amount of CNTs (**CNTs/PANI-1/32**), only polymer-capped CNTs can be seen (Figure 8c). It is interesting that the polymer shell is not smooth but looks like small fibers leaving the CNT surface. Figure 8c shows two capped CNTs linked together by polyaniline nanofibers.

The images presented in Figures 7 and 8 illustrate the mechanism of the nanocomposite formation, mainly related to the polymer growth in the two-phase dispersion. It is clear that the polymerization starts at the CNT

(59) Ping, Z.; Nauer, G. E.; Neugebauer, H.; Theiner, J.; Neckel, A. *J. Chem. Soc., Faraday Trans.* **1997**, *93*, 121–129.

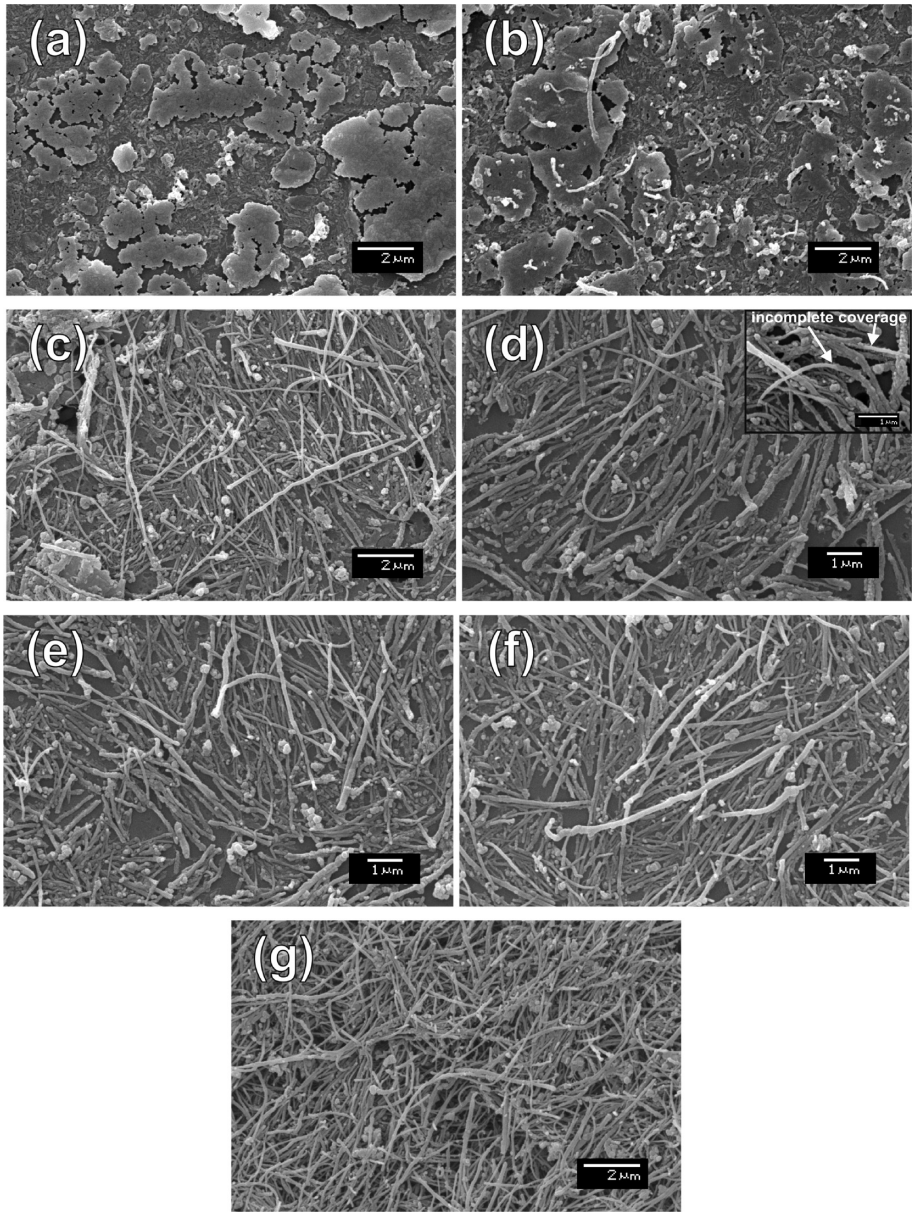

Figure 7. SEM images of the samples: (a) neat PANI; (b) **CNT/PANI-1/100**; (c) **CNT/PANI-1/32**; (d) **CNT/PANI-1/16**; (e) **CNT/PANI-1/8**; (f) **CNT/PANI-1/4**; and (g) neat CNTs.

surface and that the CNTs act as seeds for heterogeneous nucleation. When the amount of CNTs is high (and consequently the aniline is low), all the polymer growth is around the CNTs, resulting in the polymer shell observed in both the SEM and TEM images. By increasing the amount of aniline (and decreasing the proportion of CNTs), the large excess of monomer starts homogeneous nucleation, resulting in the polymer nanofiber aggregates seen in the samples containing less CNTs. We suggested this mechanism for the polyaniline/silver nanoparticle nanocomposites obtained by interfacial polymerization[43] and for polyaniline/titanium dioxide[40,41] and carbon nanotubes/polythiophene/gold nanoparticles nanocomposites,[60] both prepared in a conventional one-phase polymerization. Zhang et al. also proposed a similar mechanism to prepare polyaniline nanofibers by nanofiber seeding.[61] It is interesting that the polymer presents the nanofiber morphology in all samples, which is characteristic of interfacial polymerization and means that the presence of CNTs in the organic phase does not change the mechanism of the interfacial polymerization already proposed by Kaner et al.[36,37]

The amount of both polyaniline and carbon nanotubes in the resulting nanocomposite materials was estimated by thermogravimetric analysis. Figure 9 shows the TG curves and the first derivative of TG curves for the nanocomposite samples as well as the CNTs and PANI. Figure 9a shows the TG curve of the TFA-treated carbon nanotubes. The 62.8% weight loss observed in the 476−536 °C interval is due to the oxidation of carbon

(60) Oliveira, M. M.; Zarbin, A. J. G. *J. Phys. Chem. C* **2008**, *112*, 18783–18786.

(61) Zhang, X.; Goux, W. J.; Manohar, S. K. *J. Am. Chem. Soc.* **2004**, *126*, 4502–4503.

into gaseous carbon dioxide.[62] The residue of 37.2% is due to the iron species present in the CNT structure. The CNT oxidation temperature (T_o), defined (as recommended by Arpalli and Nikolaev[63]) as the temperature of the maximum in the mass loss rate (dm/dT_{max}), was 515 °C. The TG curve of neat PANI (Figure 9b) shows a 14% weight loss in the range of 30−300 °C, attributed to the loss of water and acid dopants. There is also a large weight loss in the 322−553 °C range, attributed to the oxidation of the skeletal polyaniline chain structure.[64]

The TG curves of the CNT/PANI nanocomposites are shown in Figure 9c−g. All curves show the presence of two weight losses in the regions of 310−530 °C and 530−630 °C, which are attributed to the oxidation of the PANI and CNTs, respectively. The CNT/PANI ratio in each sample was estimated from these data, and the values found correspond to the following (in weight percent of CNTs): 7% (**CNT/PANI-1/100**), 14% (**CNT/PANI-1/32**), 28% (**CNT/PANI-1/16**), 42% (**CNT/PANI-1/8**), and 48% (**CNT/PANI-1/4**). As we can see, the amount of CNTs increases from the sample **CNT/PANI-1/100** to **CNT/PANI-1/4**, as expected. A very interesting result obtained from the TG curves is the significant increase in the temperature of oxidation of CNTs in the nanocomposites (from 515 °C in the neat TFA-tretaed CNTs to 659, 648, 650, 660, and 592 °C in the samples **CNT/PANI-1/100**, **CNT/PANI-1/32**, **CNT/PANI-1/16**, **CNT/PANI-1/8**, and **CNT/PANI-1/4**, respectively). The increase in the T_o means that the CNTs become more stable in the nanocomposites, indicating a real interaction between the CNTs and the polyaniline.

The films of the nanocomposites were deposited on transparent electrodes and studied by cyclic voltammetry. The results are presented in Figure 10. The cyclic voltammogram of the neat CNT film does not present any response in the potential window studied, as can be seen in Figure S7, Supporting Information. The cyclic voltammogram of the neat PANI and the nanocomposite films, however, show two well-defined reversible redox processes characteristic of polyaniline, confirming that the polymer presents electroactivity: redox pairs **A**/**A′** and **D**/**D′** at approximately 0.2 and 0.81 V, due to the oxidation lecoemeraldine/emeraldine and emeraldine/pernigraniline, respectively. During voltammogram acquisition, the typical polyaniline color changes are observed in all samples, showing that the materials display electrochromism even in the presence of high amounts of CNTs (as in the sample **CNT/PANI-1/4**). According to the amount of CNT increases in the nanocomposites, the voltammograms show a clear reduction in the capacitive current, due to the increase in the conductivity of samples attributed to the presence of CNTs (as will be discussed further). Other important information was

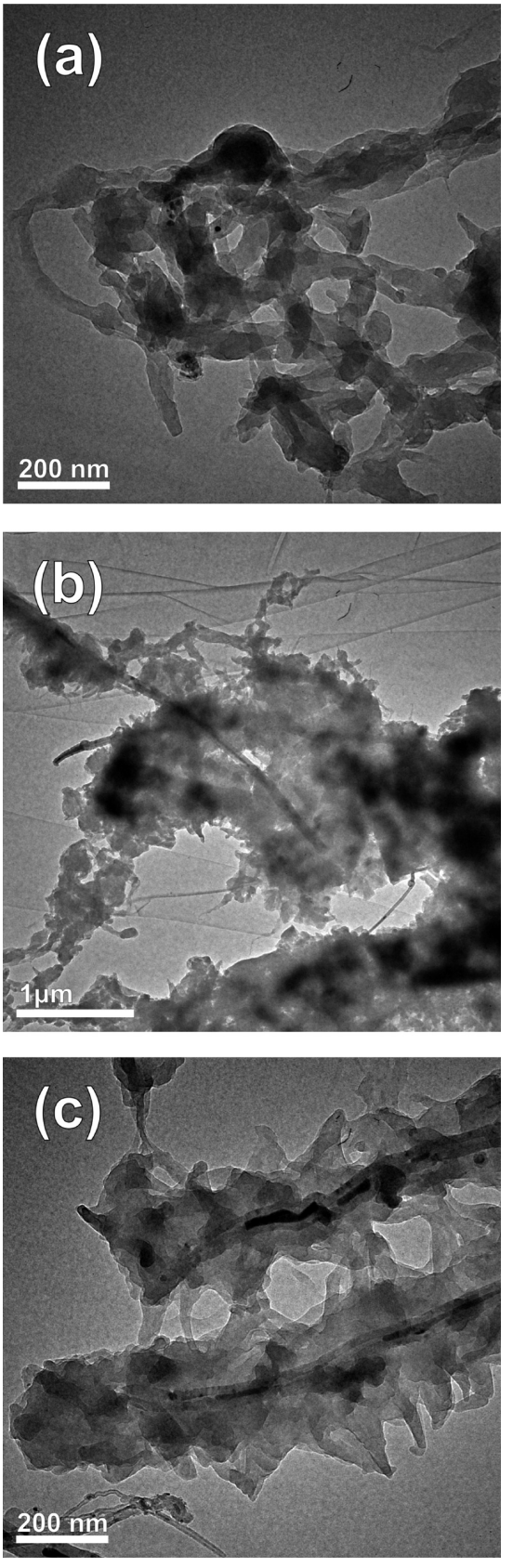

Figure 8. TEM images of the samples: (a) neat PANI; (b) **CNT/PANI-1/100**; and (c) **CNT/PANI-1/32**.

obtained from the voltammograms of the nanocomposites: (i) depending on the increase in the amount of CNTs, the oxidation peak **A** becomes thinner, indicating that the

(62) McKee, G. S. B.; Vecchio, K. S. *J. Phys. Chem. B* **2005**, *110*, 1179–1186.
(63) Arepalli, S.; Nikolaev, P.; Gorelik, O.; Hadjiev, V. G.; Holmes, W.; Files, B.; Yowell, L. *Carbon* **2004**, *42*, 1783–1791.
(64) Han, M. G.; Lee, Y. J.; Byun, S. W.; Im, S. S. *Synth. Met.* **2001**, *124*, 337–343.

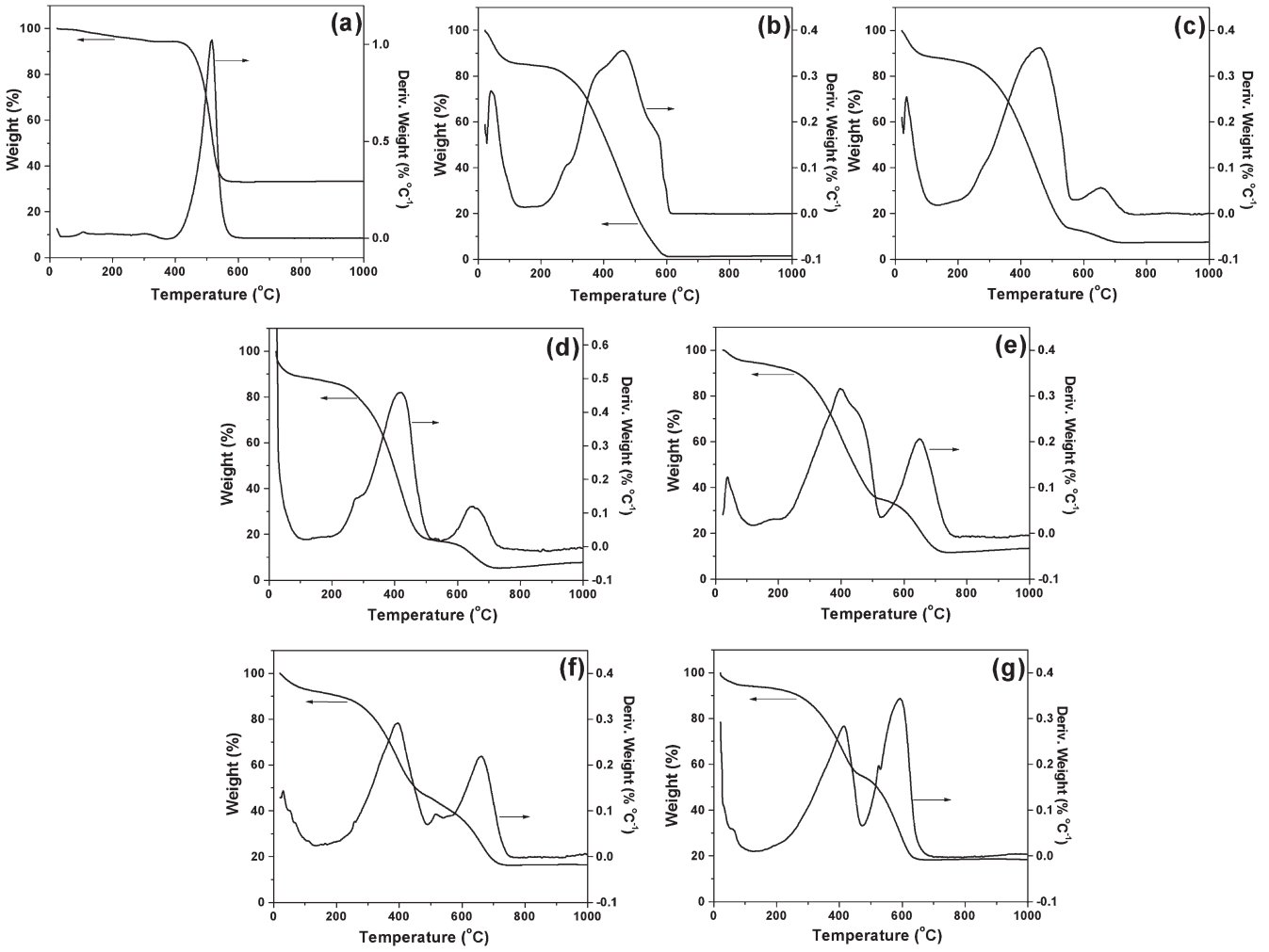

Figure 9. Thermogravimetric curves (collected in air) and first derivative of TG curves for the samples: (a) neat CNTs; (b) neat PANI; (c) **CNT/PANI-1/100**; (d) **CNT/PANI-1/32**; (e) **CNT/PANI-1/16**; (f) **CNT/PANI-1/8**; and (g) **CNT/PANI-1/4**.

leucoemeraldine/emeraldine conversion becomes easier; (ii) the potential of peak **A** is lowered by approximately 8 mV in the nanocomposites containing higher CNT amounts (in comparison to the neat PANI), which is more evidence that the incorporation of CNTs in the films facilitates the leucoemeraldine/emeraldine conversion; (iii) the current density of the peak **D** (at 0.81 V) diminishes according to the increases in the amount of CNTs, and concomitantly, another peak at 0.9 V appears and shows increasing intensity with increasing amounts of CNTs (see the arrows in voltammograms of the samples **CNT/PANI-1/16**, **CNT/PANI-1/8**, and **CNT/PANI-1/4** in Figure 10). This last feature should again be attributed to the presence of the more polaronic polyaniline chains in the presence of CNTs. Because of the increased stabilization of the polaronic structure, the oxidation to pernigraniline (peak **D**) is assumed to become more difficult, which is reflected in the increase in the potential to perform this oxidation (from 0.81 V in the neat PANI to 0.9 V in the **CNT/PANI-1/4** sample).

The electrochemical stability of the nanocomposites was evaluated performing 400 consecutive cycles in the −0.2 to 0.55-V potential window. After 400 cycles, the current density of the film of neat polyaniline decreased 8%, and the current density of the **CNT/PANI-1/4** nanocomposite decreased only 4%, showing that the presence of the CNTS also increases the electrochemical stability of the polymer by 100%.

Figure 11 shows the sheet resistivity of the films according to the amount of CNTs. As expected, significant decreases in the sheet resistance of the films were detected with the presence of CNTs. The conductivity of the pure polyaniline and the samples **CNT/PANI-1/32** and **CNT/PANI-1/4** were calculated as 0.5 S cm^{-1}, 2.1 S cm^{-1}, and 9.5 S cm^{-1}, respectively.

As described and discussed before, several characteristics and properties of the polyaniline were modulated due to the presence of the CNTs in the nanocomposites. The interface polymer/nanotube and the interaction between these components are responsible for these alterations in the properties. All of the results discussed above clearly show that a real interaction between the polymer and the CNTs occurs in the nanocomposite films described here; this interaction occurs through a charge transfer from the polymer to the CNTs. The spectroscopic (Raman, FT-IR and UV−vis) and voltammetric data show also that the polymer/CNT interaction causes a significant increase in the amount of delocalized

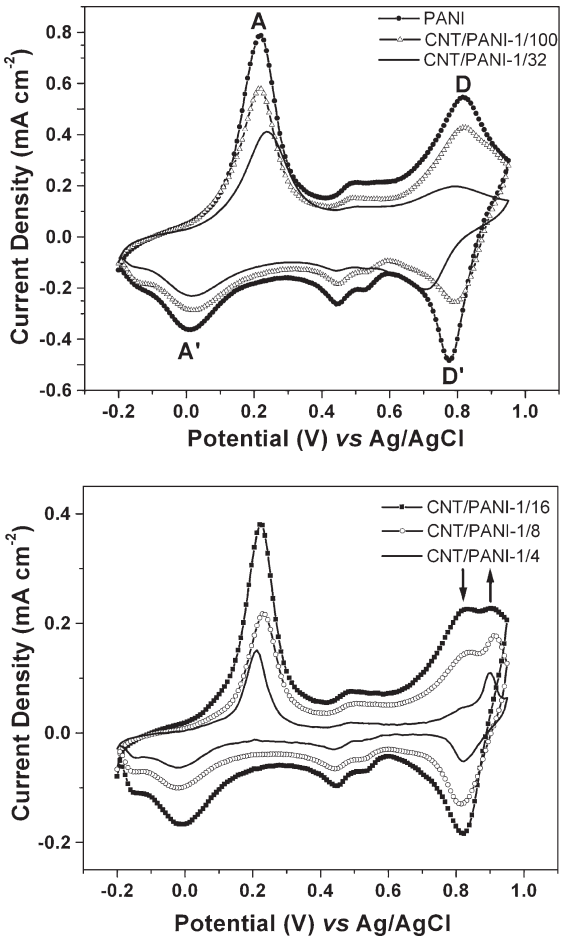

Figure 10. Cyclic voltammogram profiles (Ag/AgCl reference electrode, 0.5 mol·L^{-1} H_2SO_4 aqueous solution as the electrolyte, scan rate at 20 mV s^{-1}) for the neat polyaniline and the CNT/PANI samples.

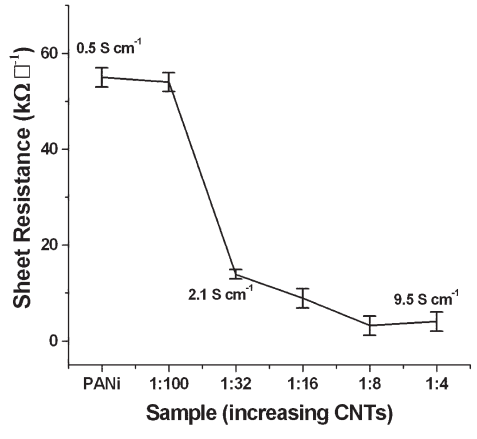

Figure 11. Curve of sheet resistance as a function of the amount of CNTs in the CNT/PANI nanocomposites. The conductivity values of the samples neat PANI, **CNT/PANI-1/32**, and **CNT/PANI-1/4** are indicated in the curve.

polarons in the polyaniline chains (accompanied by a decrease in the amount of bipolaronic units) and a change in the conformation of the chains (resulting in a more planar polyaniline). The $\pi-\pi$ aromatic interaction between the delocalized orbitals in the outside of the CNTs walls and the aromatic rings of the doped polymer is a consistent model for the system. A schematic representation of this interaction is presented in Figure 12. During the beginning of the polymerization, the polymer starts to form over the CNT wall in a typical process of heterogeneous nucleation. In order to stabilize the $\pi-\pi$ interaction, the polymer tends to grow by stacking over the CNTs, which results in more aligned and planar polymer chains around the CNTs. The polaronic structure allows for the occurrence of more planar polymer chains, and the predominance of the benzenoid rings in this kind of structure favors the $\pi-\pi$ interaction with the CNTs. In contrast, the bipolaronic structures of the PANI cause large distortions in the polymer chains. This structure favors a more angular (in contrast to a more planar) chain conformation, which means that the $\pi-\pi$ stacking would be less favorable. The occurrence of structures such as $(CNT)^{\delta-}...(PANI)^{2+}(HSO_4)^{-}{}_2$, in which the polyaniline is attracted by the delocalized electrons of the CNTs, makes the transfer of part of the electronic density from PANI to CNTs possible in a typical model in which the CNTs act as a p-dopant to the polymer.

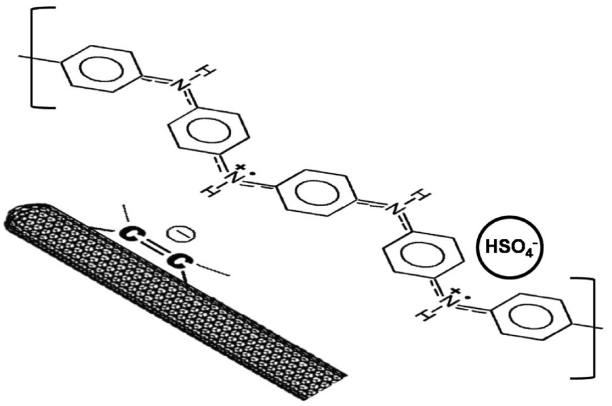

Figure 12. Proposed model for the CNT−polyaniline interaction.

As a final point, it is necessary to discuss a model for the occurrence of the freestanding films in the synthetic route described here. Some experimental evidence must be considered to understand this point. The microscopic data clearly showed that in the more concentrated CNT samples the polymer totally surrounds the CNTs, resulting in a core−shell-like structure. In the samples containing a low amount of CNTs, this core−shell-like structure is also observable, but several regions containing free polymer were also detectable. These observations indicate that the polymerization reaction starts over the dispersed CNTs and that the CNTs act as seeds in a heterogeneous reaction. If the amount of CNTs available is high, there is sufficient CNT surface area to guarantee that all of the monomer is able to polymerize around the nanotubes, yielding only CNTs capped by the polymers (as observed in the samples **CNT/PANI-1/16**, **CNT/PANI-1/8**, and **CNT/PANI-1/4**). The importance of the presence of the CNTs in the polyaniline polymerization was also confirmed through other experiments not shown here: (i) the polymerization yield (estimated by the fraction of aniline that was converted to PANI) increases according to the increases in the amount of CNTs initially dispersed in the toluene, and (ii) the presence of CNTs

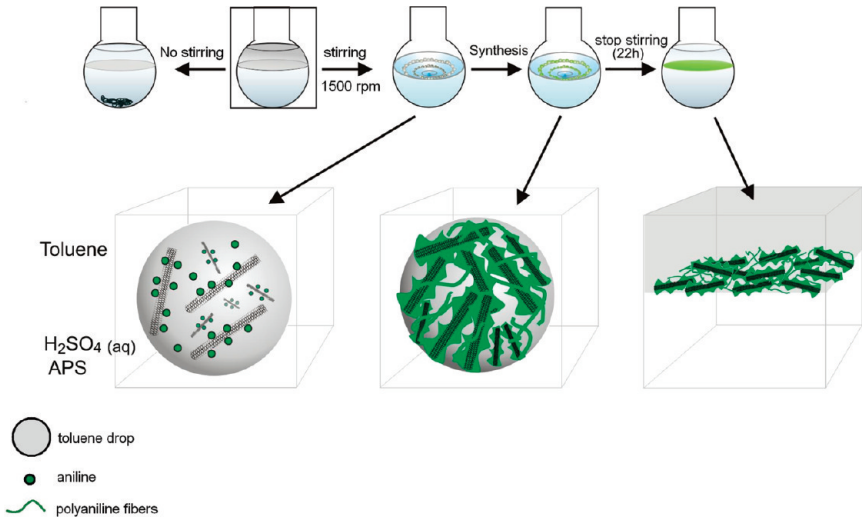

Figure 13. Schematic representation for the occurrence of CNT/polyaniline films at the water/toluene interface.

affects the polymerization kinetics (the blue and green color characteristics of the polyaniline appear more quickly with the increase in the CNTs dispersed in toluene).

Besides the real influence of the presence of dispersed CNTs in the polymerization step, another piece of important experimental data involves the stirring during the synthesis. It is well known that in order to guarantee the formation of polyaniline nanofibers through the two-phase system, the interfacial polymerization should be carried out in the absence of stirring.[38] In our system, the syntheses carried out without stirring (or with no-vigorous stirring) did not produce freestanding films but yielded a green powder deposited at the bottom of the flask. These materials were characterized and consisted of inhomogeneous PANI/CNT nanocomposites. The stirring of the system is a key point to guaranteeing the occurrence of the freestanding films at the water/toluene interface.

Finally, it is important to consider the nature of the liquid−liquid interface. Theoretical and experimental models have been proposed to understand the nature of the water molecules at the water/oil interface.[65] Some data indicate that the water molecules at interfaces resulting from liquids containing high differences in polarities (such as water/toluene) are assembled with the dipoles aligned in parallel to the interfacial plane. These molecules do not have strong interactions with the other water molecules and the present one free O−H bond in the direction of the organic phase. The occurrence of this localized field at the interface could explain the transport of molecules and ions across the phases and leads to the understanding of the so-called Pickering emulsions. Pickering was the first to describe how water/oil emulsions could be stabilized by insoluble particles.[65] Nowadays, it is accepted in the literature that the high interfacial energy at interfaces can be minimized (causing interface stabilization) by solid particles.[66−69] In order to stabilize an interface, the solid material needs be able to interact equally with both phases. This model can be employed to explain the occurrence of the films at the interface in the nanocomposite samples described in this work.

The proposed mechanism for the formation of the CNTs/PANI nanocomposite freestanding films can be summarized in Figure 13. During the stirring, small drops of toluene (containing both the CNTs and aniline) become dispersed in the aqueous solution. Gradually, the CNTs and aniline dispersed in these toluene drops migrate to the toluene/water interface, and the polymerization begins over the CNTs walls. The resulting polyaniline-capped CNTs at the interface guarantee the stabilization discussed before. When the stirring is interrupted, several toluene drops agglomerate to originate the continuum phase of toluene. Additionally, all the polyaniline-capped CNTs that were located at the interfaces of each toluene drop/water also agglomerate in a kind of net that is continuously and homogeneously located at the toluene/water interface, resulting in the self-standing films described here. In order to attest to the generality of this mechanism, similar reactions have been conducted in other oil/water systems (using chloroform as organic phase for example), under stirring, and similar CNT/polyaniline films have been obtained.

Conclusions

In conclusion, this work reports for the first time the preparation of novel carbon nanotube/polyaniline nanocomposite self-standing films in which both the synthesis and processing of the nanocomposites are performed together in one single step. These materials were prepared through a simple interfacial polymerization by controlling the aniline/CNT ratio and the stirring of the system. The presence of CNTs dramatically affects the interfacial

(65) Moore, F. G.; Richmond, G. L. *Acc. Chem. Res.* **2008**, *41*, 739–748.
(66) Pickering, S. U. *J. Chem. Soc., Trans.* **1907**, *91*, 2001–2021.
(67) Wang, D.; Duan, H.; Mohwald, H. *Soft Matter* **2005**, *1*, 412–416.
(68) Binks, B. P.; Lumsdon, S. O. *Langmuir* **2000**, *16*, 8622–8631.
(69) Binks, B. P. *Phys. Chem. Chem. Phys.* **2007**, *9*, 6298–6299.

polymerization of aniline. The aniline polymerization starts at the CNTs walls, which results in a final material in which the CNTs are capped by a fibrous polymer shell. On the basis of several characterization techniques, a model for the carbon nanotube/polyaniline interactions was discussed. Clearly, the presence of CNTs yields polyaniline chains with a more planar conformation and more polaronic structure. A model for the film formation based on the stabilization of the interfacial energy was also proposed.

Besides the description of a novel kind of material presenting obvious technological relevance (due to the potential applications of these nanocomposite films in many devices), a key point of this article was the complementary utilization of different techniques for a careful characterization of the interactions between the carbon nanotubes and the polyaniline chains, which are crucial for understanding several properties of these systems.

We believe that the interfacial synthesis presented here should be a very general route to prepare different kinds of nanocomposite materials. Some applications of these films as sensors, electrochromic materials, and sensitive materials for photovoltaic devices are currently under investigation in our group.

Acknowledgment. We gratefully acknowledge the financial support of CNPq, CAPES-PROCAD, the Brazilian Network on Carbon Nanotubes Research (CNPq), and INCT-Nanocarbono (CNPq). We also thank LME-UFPR for the TEM images. R.V.S. thanks CAPES for the fellowship.

Supporting Information Available: TEM images, X-ray diffractogram profile, XPS and TGA data for the CNTs; UV−vis spectra of the nanocomposites; and a cyclic voltammogram of the CNTs (PDF). This material is available free of charge via the Internet at http://pubs.acs.org.